It was determined that in an electrolyte containing 1.75 g/L KOH+1 g/L Na_2SiO_3+2 g/L $NaAlO_2$, with an increase in current density from 15 A/dm^2 to 50 A/dm^2, the phase composition of the coating changes. In the three-phase state (aluminum titanate, rutile, and amorphous-like phase), with increasing j, instead of an amorphous-like phase, a crystalline mullite phase appears. The hardness of the coating increases from 5400 MPa to 12500 MPa. It was found that, in combination with aluminum titanate, mullite is the basis for achieving high hardness in the coating. The formation of a ceramic micro-arc oxide coating on the surface of the VT3-1 titanium alloy makes it possible to reduce the dry friction coefficient by more than 5 times to f=0.09.

The effect of electrolysis conditions during micro-arc oxidation of the VT3-1 alloy (titanium-based) on the growth kinetics, surface morphology, phase-structural state, and physical and mechanical characteristics (hardness, coefficient of friction) of oxide coatings was studied. It was found that the process in the mode of micro-arc discharges is stably implemented on the VT3-1 alloy in an alkaline (KOH) electrolyte with additions of sodium aluminate ($NaAlO_2$) and liquid glass (Na_2SiO_3). This makes it possible to obtain coatings up to 250 μm thick. In this case, a linear dependence of the coating thickness on the time of the MAO process is observed. The growth rate of the coating increases with increasing current density. The highest growth rate was 1.13 μm/min. It was revealed that in an electrolyte containing 1 g/L KOH+14 g/L $NaAlO_2$ with an increase in the duration of oxidation from 60 to 180 minutes, the relative content of the high-temperature phase, rutile, increases. In the coatings obtained in the electrolyte 1.75 g/L KOH+1 g/L Na_2SiO_3+2 g/L $NaAlO_2$, with an increase in the duration of the MAO process, the relative content of the amorphous-like phase decreases and the content of the crystalline phase of mullite ($3Al_2O_3 \cdot 2SiO_2$) increases

Keywords: micro-arc oxidation, VT3-1, electrolyte type, growth kinetics, phase composition, wear resistance

UDC 539.216.2: 537.52
DOI: 10.15587/1729-4061.2020.214308

AN EXPERIMENTAL ANALYSIS OF THE INFLUENCE OF ELECTROLYTE COMPOSITIONS, CURRENT DENSITY AND DURATION OF THE MICRO-ARC OXIDATION PROCESS ON THE STRUCTURAL-PHASE STATE AND PROPERTIES OF VT3-1 TITANIUM ALLOY

V. Subbotina
PhD, Associate Professor*
E-mail: subbotina.valeri@gmail.com
O. Sobol'
Doctor of Physical and Mathematical Sciences, Professor*
E-mail: sool@kpi.kharkov.ua
V. Belozerov
PhD, Professor*
E-mail: belozerov.valerii@gmail.com
V. Shnayder
Postgraduate Student*
E-mail: valikshnayder@gmail.com
O. Smyrnov
PhD, Leading Researcher
Forensic Laboratory
Hon. Prof. M. S. Bokarius Kharkiv Research Institute of Forensic Examinations
Zolochivska, str., 8a, Kharkiv, Ukraine, 61177
E-mail: smirnov_alexa@ukr.net
*Department of Materials Science
National Technical University
"Kharkiv Polytechnic Institute"
Kyrpychova str., 2, Kharkiv, Ukraine, 61002

Received date 02.09.2020
Accepted date 27.09.2020
Published date 23.10.2020

1. Introduction

Plasma processes have recently become the basis of modern surface hardening technologies [1, 2]. Due to the strong disequilibrium of such processes, it is difficult to simulate them [3, 4], therefore, to predict the properties obtained as a result of plasma technologies of materials, the method of structural engineering began to be used [5, 6]. This is especially important for engineering materials, where surface properties in most cases determine their functional characteristics. In this regard, the optimization of properties based on the structural approach for this class of materials refers

mainly to the surface [7, 8]. The greatest effect of improving the properties when using this approach was the creation of ceramic-like coatings on the surface. Such coatings with high properties are based on nitrides [9, 10], borides [11, 12] and oxides [13, 14] of transition metals, both in the form of single-layer [15, 16] and multilayer [17, 18] composites.

Recently, special attention has been paid to oxide ceramic-like coatings in connection with the development of a very promising method for surface modification – micro-arc oxidation [19, 20]. The highest properties for this class of coatings were mainly achieved during the formation (both on the basis of the base material and by using special electrolytes) of a highly hard α-Al_2O_3 (corundum) phase [21, 22].

It should be noted that, as a rule, it is difficult to heat-treat the coating after micro-arc oxidation. This is due to the fact that the range of temperatures required for significant structural and phase changes in such oxides is usually higher than the melting point of the base material. Therefore, to obtain the required composition of the coating, it is necessary to change the technological conditions in the process of micro-arc oxidation. In this regard, the development of the method of structural engineering for the MAO process is of great importance. This is an urgent task in connection with the large range of alloy products for which the industrial use of MAO processing is effective. In this connection, the generalization of structural data for various types of materials is the basis for working out the MAO technology in order to optimize it.

2. Literature review and problem statement

Titanium and titanium-based alloys are important structural materials for mechanical engineering and medical equipment and are often used as elements of friction pairs. Therefore, for this class of materials, it is rather important to improve the physical and mechanical properties of the surface, which has been shown in numerous studies of the functional properties of titanium and alloys.

In particular, in [23] the need to improve the functional properties of the surface was associated with its relatively high and unstable coefficient of friction (COF), in [24] the need to increase the relatively low abrasive and adhesive wear resistance was shown. Critical properties that need to be improved for effective use of the material were also noted: relatively low hardness [25, 26], strong tendency to abrasion [27] and low load-bearing capacity [27, 28]. All of these characteristics significantly limit the use of titanium-based materials in wear technology.

This problem has become especially important in connection with the extensive use of titanium-based alloys in medicine – in the form of various types of implants [29, 30]. The titanium oxide layers, which are formed on titanium surfaces, do not have high mechanical properties and additional processing is required to form a high-temperature dense TiO_2 rutile phase [31, 32]. In this case, a relatively thin natural oxide film on titanium is easily destroyed by friction. The dry friction coefficient for a titanium-titanium pair is 0.6, which is close when tested in oil and water [33].

In addition, to ensure good adhesion of TiO_2, for example, to bone tissue, a large surface area and porosity are required (at the level of tens of microns, which is compatible with the size of the bone cell). As shown in [34], this can provide titanium oxidation in the micro-arc mode.

As shown by the studies given in [35, 36], coatings obtained as a result of micro-arc oxidation of titanium alloys can significantly increase the elastic modulus and wear resistance of the base material. In addition, such coatings have high electrical insulating characteristics [37, 38], high values of hardness and electrochemical potential [39, 40]. Moreover, such an important characteristic as wear resistance can be increased tenfold [41].

The largest number of studies on micro-arc processing of titanium alloys is associated with the Ti–6Al–4V alloy [42, 43]. It was found [44] that the treatment of the Ti (Ti–6Al–4V) alloy can lead to a significant content of the mixed oxide Al_2O_3 TiO_2 (aluminum titanate).

However, electrolytes currently used for this have a number of disadvantages. For example, the use of Ca-P electrolyte does not provide the required growth rate [45], while the H_3PO_4 electrolyte leads to an unstable process of micro-arc oxidation and its transition to arc oxidation [46].

Good results were shown by the use of alkali-aluminate electrolytes for micro-arc oxidation of titanium alloys. This made it possible to obtain hard, heat-shielding, dielectric coatings on the surface of titanium alloys [47].

However, little attention was paid to the study of the regularities of the formation of the phase composition and the quantitative ratio of the phases included in MAO coatings under various technological processing modes. Although it is the phase composition of the coating that should determine their properties.

Also, in studies devoted to the investigation of the processes of micro-arc oxidation of titanium alloys both in alkali-aluminate and alkali-silicate aqueous solutions, and in other electrolytes, the reasons for the kinetic features of the growth of coatings have not been determined. Although there is no doubt that with a change in the growth kinetics of a coating on a titanium alloy (during its MAO treatment), there is a change in the structure and phase composition of such a coating, which determine its basic properties.

3. The aim and objectives of the study

The aim of the study was to identify the effect of the electrolyte composition, current density and time of the micro-arc oxidation process on the phase-structural state and properties of coatings formed during the anodic-cathodic process on the VT3-1 titanium alloy.

To achieve the aim, the following objectives were set:

– to determine the possibility of the MAO process on the VT-1 alloy in an alkaline (KOH) electrolyte with additions of sodium aluminate ($NaAlO_2$) and liquid glass (Na_2SiO_3) and to study the growth kinetics of such coatings;

– to determine the dependence of the phase composition of MAO coatings on the oxidation time;

– to study the effect of the current density during oxidation on the phase-structural state and hardness of MAO coatings.

4. Material and method for studying the effect of the type and composition of electrolyte on the structure and properties of MAO coatings

The studies were carried out on the VT3-1 titanium alloy, the chemical composition of which is given in Table 1.

Table 1

Chemical composition of the VT3-1 titanium alloy

Main elements, %			Impurity elements, % no more					
Ti	Al	Cr	C	Fe	Si	Zr	O	N
Basis	5.5	2.5	0.10	0.30	0.15	0.30	0.20	0.05

VT3-1 is a deformed alloy with (α+β)-structure.

MAO treatment of alloys was carried out in an alkaline (KOH) electrolyte with additions of sodium aluminate ($NaAlO_2$) and liquid glass (Na_2SiO_3, ρ≈1.4 g/cm^3).

Thus, 2 types of electrolytes were used:

1) 1.4 g/L KOH+14 g/L $NaAlO_2$ (solution in distilled water). For this series of samples, the current density during electrolysis was j=20–40 A/dm^2, and the duration of the process for studying the growth kinetics and the phase formation process was τ=1, 2, and 3 hours.

2) 1.75 g/L KOH+1 g/L Na_2SiO_3+2 g/L $NaAlO_2$ (solution in distilled water). For this series of samples, the current density during electrolysis was j=15, 25, and 50 A/dm^2, and the duration of the process for studying the kinetics of growth and the process of phase formation was τ=1, 2, and 3 hours.

A capacitor-type power supply with a power of 40 kW was used.

Determination of the phase composition of MAO coatings was carried out according to the results of X-ray phase analysis. The studies were carried out on a DRON-3 setup (Burevestnik, Russia) in monochromatic $K_α$–Cu radiation. Diffraction spectra were recorded using the Bragg-Brentano reflection scheme [48]. The survey was carried out both in continuous and pointwise mode with a step of 2θ=0.1°. The maximum error in determining the content of structural crystalline components (with a detectability of 10 vol. %) does not exceed ±0.7 %. The minimum detectability of structural components is about 1 vol. %.

The results obtained in the study refer to the main coating layer (the technological layer was removed by cleaning on abrasive paper).

For quantitative phase analysis, the method of reference mixtures was used [49]. For this, calibration graphs of the dependence of the intensities of the comparison lines on the mixture composition were constructed. The basic components of the coating composition were TiO_2 (anatase, ASTM Card File 21-1272), TiO_2 (rutile, ASTM Card File 21-1276), mullite ($3Al_2O_3$ $2SiO_2$, ASTM Card File 15-776) and aluminum titanate ($TiAl_2O_5$, ASTM Card File 26-40). If peaks from the titanium substrate appeared in the diffraction spectra, they were not taken into account when calculating the coating composition.

The coating thickness was determined on a VT-10 NTs vortex thickness gauge (Kontrolpribor, Russia).

The microhardness was determined using a PMT-3 device (AO LOMO, Russia).

5. Results of studying the growth kinetics, morphology, phase-structural state, and properties of MAO coatings on VT8-1 alloy

5. 1. Surface morphology and kinetics of coating growth

The surface morphology of titanium alloy samples after MAO treatment is shown in Fig. 1.

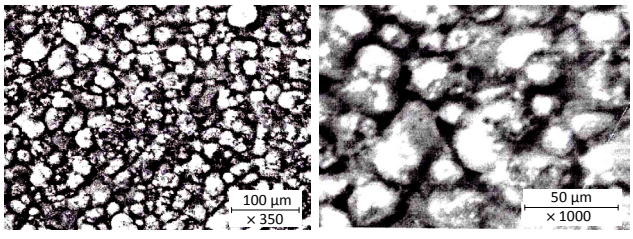

a *b*

Fig. 1. Surface morphology of coatings on the VT-3-1 alloy: *a* – general view of the surface (magnification ×350); *b* – enlarged view of the structure of "vesicular" formations on the surface (magnification ×1000)

It is seen that after microplasma oxidation, a "vesicular" surface is formed (Fig. 1, *b*). These "vesicular" formations correspond to the sections of the plasma channels of plasma breakdown with the formation of a ceramic oxide phase [50].

Three layers are clearly visible on the side cut of the VT3-1 alloy after MAO treatment (Fig. 2). The first lowest layer refers to the base metal of the VT3-1 alloy. The second layer (base coat) consists of dense crystalline ceramic components of the MAO coating and is the main functional layer. The third (surface) layer consists of loose (usually amorphous-like) structural components, has a "vesicular" structure and is a technological layer that can be easily removed after the MAO process.

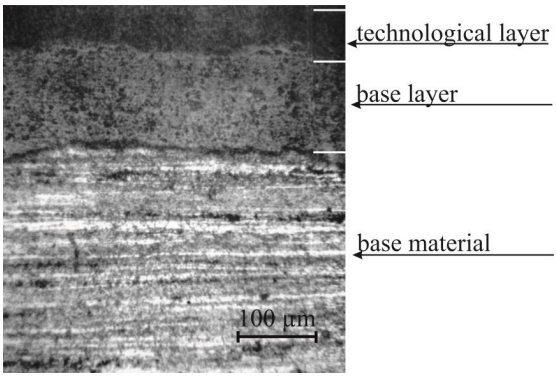

Fig. 2. Microstructure of the side surface of the section of the VT3-1 alloy after MAO treatment

To determine the kinetic characteristics of the coating growth for all series of coatings, the dependences of the thickness of the coatings on the time of the MAO process were plotted (Fig. 3, 4).

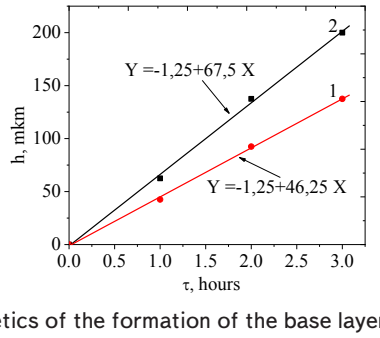

Fig. 3. Kinetics of the formation of the base layer thickness of the coating on the VT3-1 alloy (electrolyte composition 1.4 g/L KOH+14 g/L $NaAlO_2$) at different current densities: 1 – j=20 A/dm^2, 2 – j=40 A/dm^2

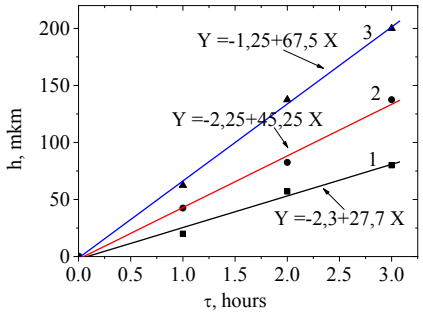

Fig. 4. Kinetics of the formation of the base layer thickness of the coating on the VT3-1 alloy (electrolyte composition 1.75 g/L KOH+1 g/L Na_2SiO_3+2 g/L $NaAlO_2$) at different current densities: 1 – j=15 A/dm^2, 2 – j=25 A/dm^2, 3 – j=50 A/dm^2

As can be seen from Fig. 3, 4, there is a linear dependence of the coating thickness on the processing time, i. e., it is determined by the amount of electricity passed. With an increase in the current density, the growth rate of the coating on the VT3-1 alloy increases.

In order to determine the growth rate, the obtained values were linearized by first-order polynomials, the equations of which are shown in Fig. 3 and 4 near each of the graphs. Based on the obtained dependences, the growth rates of coatings were calculated at different current densities.

Based on the obtained dependences, the kinetic factor (coating growth rate V) in the electrolyte 1.4 g/L KOH+14 g/L $NaAlO_2$ changes from $V_{20A/dm2}$=0.77 μm/min to $V40_{A/dm2}$=1.13 μm/min. Thus, with a twofold increase in the current density in the electrolyte 1.4 g/L KOH+14 g/L $NaAlO_2$, the growth rate increases 1.48 times.

In the electrolyte 1.75 g/L KOH+1 g/L Na_2SiO_3+2 g/L $NaAlO_2$, the growth rate also changes depending on the current density (Fig. 4). Thus, with an increase in the current density from 15 A/dm^2 to 50 A/dm^2, the growth rate changes from $V_{15A/dm2}$=0.45 μm/min and $V_{25A/dm2}$=0.77 μm/min to $V_{50A/dm2}$=1.13 μm/min. Thus, with an increase in the current density from 15 A/dm^2 to 50 A/dm^2, the growth rate of the coating increases more than 2 times. Thus, if we compare the growth rate in two different electrolytes, then the high content of $NaAlO_2$ in the first electrolyte increases the relative deposition rate of the coating.

For a visual representation of the change in the growth kinetics of MAO coatings with increasing current density for different times of the process, the dependences $h=f(j)$ are of interest. These dependences are shown in Fig. 5, where the dependences both for the total thickness (taking into account the technological layer, dependence 2), and for the base layer of the coating (dependence 1) are presented in comparison.

From the obtained dependences, it is possible to estimate the growth kinetics of coatings on the current density for the process duration of 1 and 3 hours. With the process duration of 1 hour (Fig. 5, *a*) in the range of current densities j=(15–50) A/dm^2, the dependence of the growth rate on the current density for the total coating thickness is 1.38 μm/(A/dm^2), and the growth rate of the base layer is 1.23 μm/(A/dm^2). With the process duration of 3 hours (Fig. 5, *b*) in the current density range j=(15–50) A/dm^2, the dependence of the growth rate on the current density for the total coating thickness is 3.62 μm/(A/dm^2), and the growth rate of the base layer is 4.77 μm/(A/dm^2). Thus, with an increase in the process duration, the current density becomes an increasingly significant factor in increasing the growth rate. In this case, the influence of the current density has the greatest effect on the growth rate of the base layer (Fig. 5, *b*, dependence 1). Apparently, this is due to a higher temperature in the plasma micro-arc with an increase in the coating thickness during growth for 3 hours, compared with a similar value with a shorter process duration of 1 hour.

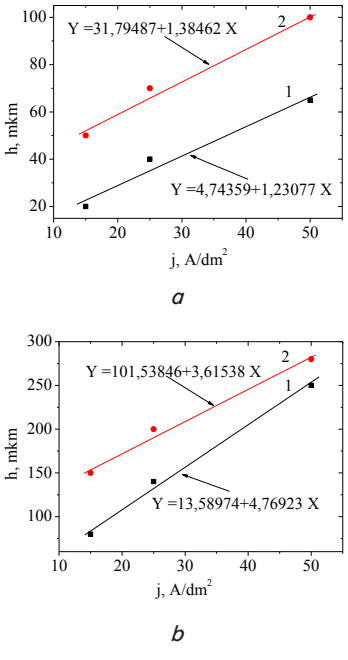

Fig. 5. Dependences of the MAO coating thickness on the current density during the MAO process (electrolyte 1.75 g/L KOH+1 g/L Na_2SiO_3+2 g/L $NaAlO_2$): 1 – base layer thickness, 2 – total MAO coating thickness (taking into account the technological layer). Duration of the process: *a* – τ=1 hour; *b* – τ=3 hours

Also, from the presented data obtained in Fig. 5 results it can be seen that with an increase in the duration of the MAO process, the relative contribution of the technological layer to the total thickness of the coating decreases. This may be due to an increase in discharge power with an increase in coverage [51].

5. 2. Phase composition of oxide coatings obtained by changing the oxidation time and different electrolyte compositions

As is known, the properties of MAO coatings are determined by their phase-structural state [51, 52]. To determine the phase-structural state of MAO coatings, X-ray diffractometry was used.

X-ray analysis showed that the coatings on titanium alloys are mainly crystalline.

During electrolysis using 1.4 g/L KOH electrolyte+ +14 g/L $NaAlO_2$, a 3-phase state is formed in the coating (base layer): anatase, rutile, and aluminum titanate (Fig. 6).

The phase ratio in the coating changes with the duration of the MAO process and is practically independent of the current density. Fig. 7 shows the dependences of the phase composition for different durations of oxidation at a current density j=40 A/dm^2. It is seen that with an increase in the duration of oxidation, the ratio of the crystalline phases of

rutile and aluminum titanate mainly changes (the relative content of rutile increases and the content of aluminum titanate decreases).

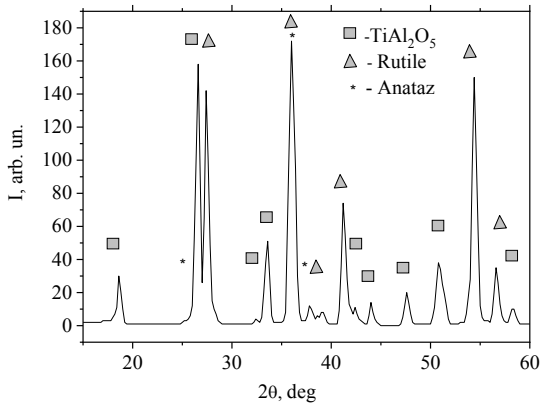

Fig. 6. Fragment of the diffractogram of the VT3-1 alloy after MAO treatment in the electrolyte 1.4 g/L KOH+14 g/L $NaAlO_2$ (τ=3 hours)

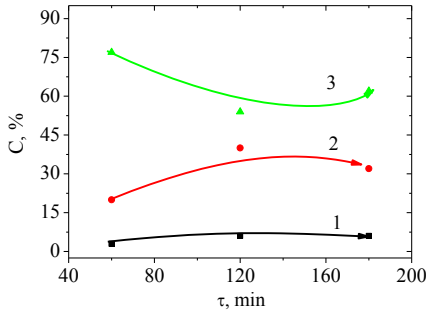

Fig. 7. Effect of oxidation duration on the phase composition of the coating (electrolyte 1.4 g/L KOH+14 g/L $NaAlO_2$): 1 – anatase, 2 – rutile, 3 – aluminum titanate

The phase composition and structural state of coatings formed in an electrolyte with the addition of liquid glass largely depend on the modes of the MAO process. The composition of such an electrolyte during the electrolysis of a titanium alloy included: 1.75 g/L KOH+1 g/L Na_2SiO_3+2 g/L $NaAlO_2$. As studies have shown, such a dependence is reflected in the fact that at a low current density j=15 A/dm^2, an amorphous-like phase appears as one of the coating components (Fig. 8, *a*). With an increase in the current density, changes occur in the phase composition of MAO coatings: instead of an amorphous-like phase, mullite ($3Al_2O{\cdot}2SiO_2$) appears as a component. The diffraction spectrum of such a coating is shown in Fig. 8, *b*.

Note that in the coatings under study, regardless of the treatment time and current density, anatase is not detected. The addition of liquid glass (Na_2SiO_3) to the electrolyte at a low flow density leads to the formation of an amorphous-like phase, and at a large one leads to the formation of mullite ($3Al_2O_3{\cdot}2SiO_2$).

In Fig. 9, the change in the phase composition of coatings from the time of the MAO process for three values of the current density during electrolysis in an electrolyte of 1.75 g/L KOH+1 g/L Na_2SiO_3+2 g/L $NaAlO_2$ is compared. As can be seen, the main trend characteristic of all values of j is an increase in the content of rutile with an increase in the duration of the process.

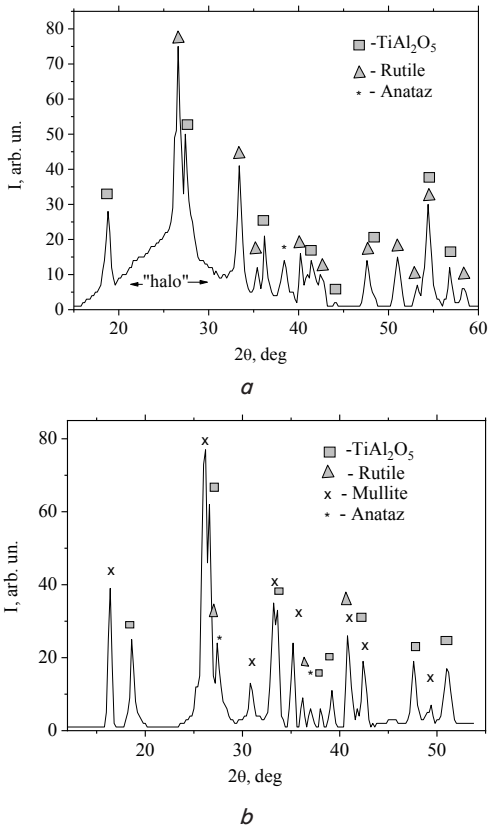

Fig. 8. Areas of X-ray diffraction spectra of MAO coatings obtained in an electrolyte solution of 1.75 g/L KOH+1 g/L Na_2SiO_3+2 g/L $NaAlO_2$ at a current density: *a* – j=15 A/dm^2 (τ=hour); *b* – j=25 A/dm^2 (τ=3 hours)

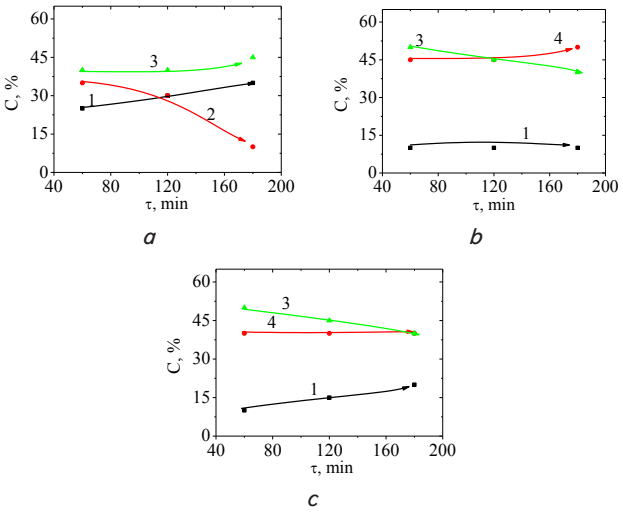

Fig. 9. Effect of oxidation duration (electrolyte 1.75 g/L KOH+1 g/L Na_2SiO_3+2 g/L $NaAlO_2$) on the phase composition of the coating at a current density: *a* – j=15 A/dm^2; *b* – j=25 A/dm^2; *c* – j=50 A/dm^2; 1 – rutile, 2 – amorphous-like phase, 3 – aluminum titanate, 4 – mullite

Thus, it has been shown that the MAO technology makes it possible to form oxide coatings of different phase composition by changing the electrolysis conditions (electrolyte composition, current density, processing time).

Note that the specific volume of the formed oxides exceeds the volume of the base on which it is formed. So, for TiO_2 $V_{ox}/V_{met.}$≈1.8; for Al_2TiO_5 – $V_{ox}/V_{met.}$≈4.4; for mullite – $V_{ox}/V_{met.}$≈13.9. This factor contributes to the formation of continuous coatings.

5. 3. Hardness and tribotechnical characteristics of MAO coatings on VT3-1 alloy

An important characteristic of the mechanical properties of MAO coatings is their hardness.

Fig. 10 shows the distribution of hardness over the thickness of the coating. A slight decrease in hardness is observed when approaching the coating surface. This can be explained by an increase in the porosity of the surface layer in comparison with deeper layers, since no changes in the phase composition were revealed.

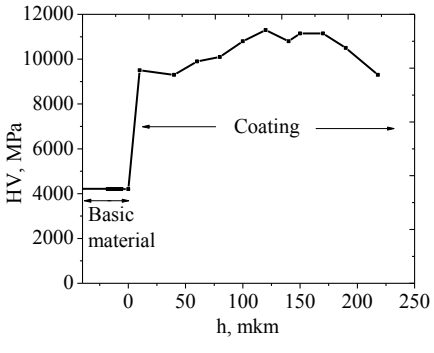

a

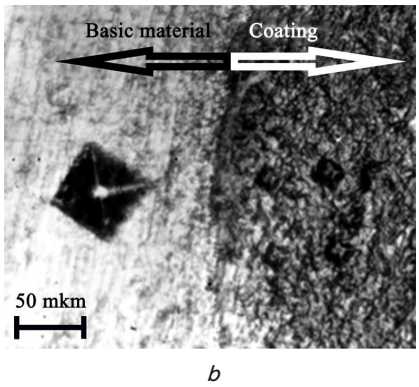

b

Fig. 10. Distribution of microhardness over the thickness of the oxide coating of the VT3-1 alloy processed by micro-arc oxidation (electrolyte 1.75 g/L KOH+1 g/L Na_2SiO_3+2 g/L $NaAlO_2$, j=50 A/dm^2, τ=3 hours): *a* – dependence of the microhardness in the "base material – coating" transition region; *b* – snapshot of the side surface of the "base material – coating" transition after indentation

It should be noted that the highest hardness of coatings obtained by MAO treatment of the VT3-1 alloy in an electrolyte solution of 1.4 g/L KOH+14 g/L $NaAlO_2$ does not exceed 6500 MPa.

The change in the hardness of MAO coatings obtained in the electrolyte 1.75 g/L KOH+1 g/L Na_2SiO_3+2 g/L $NaAlO_2$ under different technological conditions of deposition is shown in Fig. 11.

As can be seen from the results presented in Fig. 11, a large increase in the hardness of MAO coatings is observed at j=25 A/dm^2. In the case of relatively thin coatings (about 45 μm, at τ=1 hour), the hardness reaches 10,000 MPa (Fig. 11, *a*), and with a larger thickness (about 145 μm, at τ=3 hours), the hardness reaches the highest values of 12,500 MPa (Fig. 11, *b*). If we compare these parameters with the data on the phase composition of such coatings, we see (Fig. 9) that, under these conditions, crystalline mullite is formed in the coatings instead of an amorphous-like phase (at low hardness).

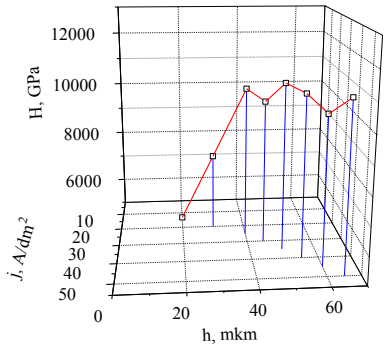

a

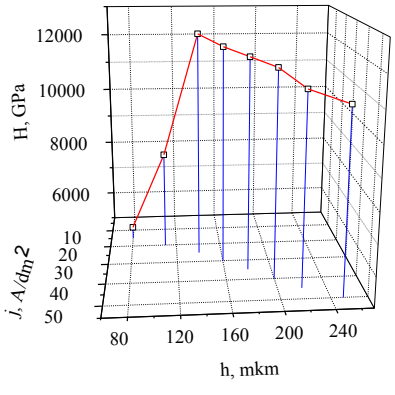

b

Fig. 11. Dependences of the hardness of MAO coatings (electrolyte: 1.75 g/L KOH+1 g/L Na_2SiO_3+2 g/L $NaAlO_2$) on the current density during oxidation and the thickness of the formed base layer: *a* – oxidation duration τ=1 hour; *b* – oxidation duration τ=3 hours

The antifriction (tribotechnical) characteristics of the hardest coatings were estimated from the value of the friction coefficient under step loading in the load range 0.12–2 kN. Wear tests were carried out on an SMTs-2 friction machine according to the disk-block scheme. The research results are shown in Fig. 12.

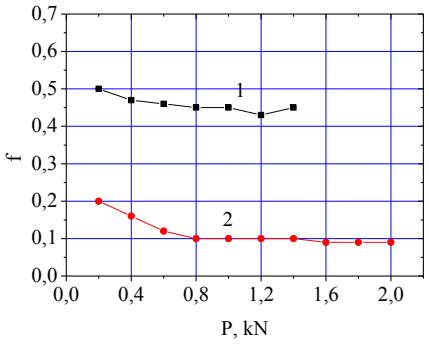

Fig. 12. Dependence of the coefficient of friction on the load for friction pairs: 1 – "VT3-1 alloy – SCH20 gray cast iron", 2 – "VT3-1 alloy with MAO-coating – SCH20 gray cast iron"

As can be seen from the results obtained, the formation of a ceramic micro-arc oxide coating on the surface of the VT3-1 titanium alloy makes it possible to reduce the dry friction coefficient by more than 5 times. In this case, the effect increases with increasing test load.

6. Discussion of the results of the effect of electrolysis conditions on the growth kinetics, phase-structural state, and properties of MAO coatings

As it was found in this study, it is possible to achieve high functional properties of the surface using the method of micro-arc oxidation. In this case, in a relatively short time (about 180 minutes), a hardening coating with a thickness of up to 250 μm can be formed on the surface (Fig. 3–5).

The phase composition and structure of such coatings, obtained by micro-arc oxidation of the VT3-1 alloy, depend not only on the composition of the electrolyte, but also on the current density and time of the oxidation process (Fig. 6–9). This is explained by an increase in the density of the energy released in the discharge and, accordingly, a higher temperature of the process.

This allows, in addition to the standard titanium oxide phases (rutile and anatase), to obtain new phase states in the coating, for example, aluminum titanate and mullite.

Thus, the production of oxide layers in a micro-arc discharge plasma allows expanding the class of formed oxide phases and their structural states. This makes it possible to fundamentally change the properties of titanium alloys, since the thickness of such oxide layers during oxidation in air is relatively small (up to 10 μm) and such coatings have a low hardness.

As was shown, as a result of using sodium aluminate ($NaAlO_2$) in the electrolyte during the MAO process, it is possible to obtain aluminum titanate (Al_2TiO_5) in the coating, which can be seen in Fig. 6, 7. This makes it possible to achieve a hardness of 6500 MPa in such coatings.

However, the greatest effect can be achieved when using a combined electrolyte containing, in addition to alkali (KOH, which increases the oxidizing ability of the electrolyte) and sodium aluminate (which supplies the coating material), also water glass Na_2SiO_3. At the same time, this use is not only due to the standard applying of a substance as a reflowing coating [50], but also allows the formation of new phases containing silicon. At low currents, the thermodynamics of the process, apparently, does not allow the formation of a crystalline phase and, as studies have shown, an X-ray amorphous phase is formed (Fig. 8, *a*). However, at a high current density, it is possible to achieve regimes in which, instead of the X-ray amorphous phase, the formation of a crystalline mullite phase occurs (Fig. 8, *b*, 9, *b*, *c*). In this case, a high-hardness state with a hardness of about 12000 MPa is achieved.

The results of studies of the effect of the phase composition on the hardening of titanium alloys indicate that it is necessary to use electrolytes that ensure the formation of a coating containing a large amount of the Al_2TiO_5 phase – aluminum titanate and mullite.

The formation of a ceramic oxide coating of high hardness (12,000 MPa) on the surface of a titanium alloy can significantly reduce the coefficient of surface friction. For example, in the tribological pair "VT3-1 alloy with MAO-coating – gray cast iron SCH20 GOST 1412-85", the dry friction coefficient can be reduced by more than 5 times and reaches f=0.09.

However, the use of such micro-arc oxidation for parts of heavily loaded friction pairs requires the achievement of a more uniform surface morphology in MAO coatings on titanium alloys and an increase in tribological characteristics. Therefore, in further studies to improve the tribological properties of the surface, it is proposed to test other components, for example, rutile $(NaPO_3)_6$ [51] in the electrolyte.

7. Conclusions

1. It was found that the MAO process in the micro-arc discharge mode is stably implemented on the VT3-1 alloy in an alkaline (KOH) electrolyte with additions of sodium aluminate ($NaAlO_2$) and liquid glass (Na_2SiO_3). This makes it possible to obtain coatings up to 250 μm thick. In this case, a linear dependence of the coating thickness on the time of the MAO process is observed. It was determined that the growth rate of the coating increases with an increase in the current density (an increase in the current density by 2 times leads to an increase in the growth rate by about 1.5 times). The highest growth rate was 1.17 μm/min.

2. It was revealed that in an electrolyte containing 1 g/L KOH+14 g/L $NaAlO_2$ with an increase in the oxidation duration from 60 to 180 minutes, the relative content of the high-temperature phase – rutile, increases. In the coatings obtained in the electrolyte 1.75 g/L KOH+1 g/L Na_2SiO_3+2 g/L $NaAlO_2$, with an increase in the duration of the MAO process, the relative content of the amorphous-like phase decreases and the content of the crystalline phase of mullite ($3Al_2O_3{\cdot}2SiO_2$) increases.

3. It was determined that in an electrolyte containing 1.75 g/L KOH+1 g/L Na_2SiO_3+2 g/L $NaAlO_2$, with an increase in the current density from 15 A/dm^2 to 50 A/dm^2, the phase composition of the coating changes. At a low current of 15 A/dm^2, a three-phase state is formed (aluminum titanate, rutile, and an amorphous-like phase). An increase in j to 50 A/dm^2 leads to the appearance of a crystalline mullite phase instead of an amorphous-like phase. In this case, the hardness of the coating increases from 5,400 MPa to 12,500 MPa.

Acknowledgments

The authors would like to express their gratitude to the Ministry of Education and Science of Ukraine for financial support within the framework of the projects "Development of materials science bases for the use of high-performance ion-plasma technologies for three-level surface engineering" (state registration number No. 0118U002044) and "Development of materials science bases for structural engineering of pseudoalloys based on Cu and Al" (state registration number No. 0119U002567).

References

1. Vereschaka, A., Tabakov, V., Grigoriev, S., Sitnikov, N., Milovich, F., Andreev, N. et. al. (2020). Investigation of the influence of the thickness of nanolayers in wear-resistant layers of Ti-TiN-(Ti,Cr,Al)N coating on destruction in the cutting and wear of carbide cutting tools. Surface and Coatings Technology, 385, 125402. doi: https://doi.org/10.1016/j.surfcoat.2020.125402

2. Sobol', O. V., Meilekhov, A. A. (2018). Conditions of Attaining a Superhard State at a Critical Thickness of Nanolayers in Multiperiodic Vacuum-Arc Plasma Deposited Nitride Coatings. Technical Physics Letters, 44 (1), 63–66. doi: https://doi.org/10.1134/s1063785018010224
3. Sobol, O., Meylekhov, A., Postelnyk, A. (2018). Computer Simulation of the Processes of Mixing in Multilayer Nitride Coatings with Nanometer Period. Advances in Design, Simulation and Manufacturing, 146–155. doi: https://doi.org/10.1007/978-3-319-93587-4_16
4. Mayrhofer, P. H., Mitterer, C., Hultman, L., Clemens, H. (2006). Microstructural design of hard coatings. Progress in Materials Science, 51 (8), 1032–1114. doi: https://doi.org/10.1016/j.pmatsci.2006.02.002
5. Sobol', O. V., Andreev, A. A., Gorban', V. F. (2016). Structural Engineering of Vacuum-ARC Multiperiod Coatings. Metal Science and Heat Treatment, 58 (1-2), 37–39. doi: https://doi.org/10.1007/s11041-016-9961-3
6. Sobol, O. V., Postelnyk, A. A., Meylekhov, A. A., Andreev, A. A., Stolbovoy, V. A. (2017). Structural Engineering of the Multilayer Vacuum Arc Nitride Coatings Based on Ti, Cr, Mo and Zr. Journal of Nano- and Electronic Physics, 9 (3), 03003-1–03003-6. doi: https://doi.org/10.21272/jnep.9(3).03003
7. Liu, Y., Wan, H., Zhang, H., Chen, J., Fang, F., Jiang, N. et. al. (2020). Engineering Surface Structure and Defect Chemistry of Nanoscale Cubic Co3O4 Crystallites for Enhanced Lithium and Sodium Storage. ACS Applied Nano Materials, 3 (4), 3892–3903. doi: https://doi.org/10.1021/acsanm.0c00614
8. Pogrebnjak, A. D., Beresnev, V. M., Bondar, O. V., Abadias, G., Chartier, P., Postol'nyi, B. A. et. al. (2014). The effect of nanolayer thickness on the structure and properties of multilayer TiN/MoN coatings. Technical Physics Letters, 40 (3), 215–218. doi: https://doi.org/10.1134/s1063785014030092
9. Sobol', O. V., Andreev, A. A., Gorban', V. F., Stolbovoy, V. A., Melekhov, A. A., Postelnyk, A. A. (2016). Possibilities of structural engineering in multilayer vacuum-arc ZrN/CrN coatings by varying the nanolayer thickness and application of a bias potential. Technical Physics, 61 (7), 1060–1063. doi: https://doi.org/10.1134/s1063784216070252
10. Mareus, R., Mastail, C., Anğay, F., Brunetière, N., Abadias, G. (2020). Study of columnar growth, texture development and wettability of reactively sputter-deposited TiN, ZrN and HfN thin films at glancing angle incidence. Surface and Coatings Technology, 399, 126130. doi: https://doi.org/10.1016/j.surfcoat.2020.126130
11. Sobol, O. V., Dub, S. N., Pogrebnjak, A. D., Mygushchenko, R. P., Postelnyk, A. A., Zvyagolsky, A. V., Tolmachova, G. N. (2018). The effect of low titanium content on the phase composition, structure, and mechanical properties of magnetron sputtered WB2-TiB2 films. Thin Solid Films, 662, 137–144. doi: https://doi.org/10.1016/j.tsf.2018.07.042
12. Moscicki, T., Psiuk, R., Słomińska, H., Levintant-Zayonts, N., Garbiec, D., Pisarek, M. et. al. (2020). Influence of overstoichiometric boron and titanium addition on the properties of RF magnetron sputtered tungsten borides. Surface and Coatings Technology, 390, 125689. doi: https://doi.org/10.1016/j.surfcoat.2020.125689
13. Zavareh, M. A., Sarhan, A. A. D. M., Razak, B. B. A., Basirun, W. J. (2014). Plasma thermal spray of ceramic oxide coating on carbon steel with enhanced wear and corrosion resistance for oil and gas applications. Ceramics International, 40 (9), 14267–14277. doi: https://doi.org/10.1016/j.ceramint.2014.06.017
14. Bajat, J. B., Vasilić, R., Stojadinović, S., Mišković-Stanković, V. (2013). Corrosion Stability of Oxide Coatings Formed by Plasma Electrolytic Oxidation of Aluminum: Optimization of Process Time. CORROSION, 69 (7), 693–702. doi: https://doi.org/10.5006/0859
15. Duan, L., Wu, H., Guo, L., Xiu, W., Yu, X. (2020). The effect of phase on microstructure and mechanical performance in TiAlN and TiSiN films. Materials Research Express, 7 (6), 066401. doi: https://doi.org/10.1088/2053-1591/ab96f6
16. Sobol', O. V., Andreev, A. A., Stolbovoi, V. A., Fil'chikov, V. E. (2012). Structural-phase and stressed state of vacuum-arc-deposited nanostructural Mo-N coatings controlled by substrate bias during deposition. Technical Physics Letters, 38 (2), 168–171. doi: https://doi.org/10.1134/s1063785012020307
17. Sobol, O. V., Andreev, A. A., Gorban, V. F., Meylekhov, A. A., Postelnyk, H. O., Stolbovoy, V. A. (2016). Structural Engineering of the Vacuum Arc ZrN/CrN Multilayer Coatings. Journal of Nano- and Electronic Physics, 8 (1), 01042-1–01042-5. doi: https://doi.org/10.21272/jnep.8(1).01042
18. Wang, T., Zhang, J., Li, Y., Gao, F., Zhang, G. (2019). Self-lubricating TiN/MoN and TiAlN/MoN nano-multilayer coatings for drilling of austenitic stainless steel. Ceramics International, 45 (18), 24248–24253. doi: https://doi.org/10.1016/j.ceramint.2019.08.136
19. Kharanagh, V. J., Sani, M. A. F., Rafizadeh, E. (2013). Effect of current frequency on coating properties formed on aluminised steel by plasma electrolytic oxidation. Surface Engineering, 30 (3), 224–228. doi: https://doi.org/10.1179/1743294413y.0000000190
20. Belozerov, V., Sobol, O., Mahatilova, A., Subbotina, V., Tabaza, T. A., Al-Qawabeha, U. F., Al-Qawabah, S. M. (2017). The influence of the conditions of microplasma processing (microarc oxidation in anodecathode regime) of aluminum alloys on their phase composition. Eastern-European Journal of Enterprise Technologies, 5 (12 (89)), 52–57. doi: https://doi.org/10.15587/1729-4061.2017.112065
21. Subbotina, V., Al-Qawabeha, U. F., Belozerov, V., Sobol, O., Subbotin, A., Tabaza, T. A., Al-Qawabah, S. M. (2019). Determination of influence of electrolyte composition and impurities on the content of α-Al_2O_3 phase in MAO-coatings on aluminum. Eastern-European Journal of Enterprise Technologies, 6 (12 (102)), 6–13. doi: https://doi.org/10.15587/1729-4061.2019.185674
22. Arbuzova, S. S., Butyagin, P. I., Bol'shanin, A. V., Kondratenko, A. I., Vorob'ev, A. V. (2020). Microarc Oxidation of Metal Surfaces: Coating Properties and Applications. Russian Physics Journal, 62 (11), 2086–2091. doi: https://doi.org/10.1007/s11182-020-01950-7
23. Yetim, A. F., Celik, A., Alsaran, A. (2010). Improving tribological properties of Ti6Al4V alloy with duplex surface treatment. Surface and Coatings Technology, 205 (2), 320–324. doi: https://doi.org/10.1016/j.surfcoat.2010.06.048

24. Budinski, K. G. (1991). Tribological properties of titanium alloys. Wear, 151 (2), 203–217. doi: https://doi.org/10.1016/0043-1648(91)90249-t
25. Yetim, A. F., Yildiz, F., Vangolu, Y., Alsaran, A., Celik, A. (2009). Several plasma diffusion processes for improving wear properties of Ti6Al4V alloy. Wear, 267 (12), 2179–2185. doi: https://doi.org/10.1016/j.wear.2009.04.005
26. Niinomi, M. (2003). Recent research and development in titanium alloys for biomedical applications and healthcare goods. Science and Technology of Advanced Materials, 4 (5), 445–454. doi: https://doi.org/10.1016/j.stam.2003.09.002
27. Qin, L., Liu, C., Yang, K., Tang, B. (2013). Characteristics and wear performance of borided Ti6Al4V alloy prepared by double glow plasma surface alloying. Surface and Coatings Technology, 225, 92–96. doi: https://doi.org/10.1016/j.surfcoat.2013.02.053
28. De Viteri, V. S., Barandika, M. G., de Gopegui, U. R., Bayón, R., Zubizarreta, C., Fernández, X. et. al. (2012). Characterization of Ti-C-N coatings deposited on Ti6Al4V for biomedical applications. Journal of Inorganic Biochemistry, 117, 359–366. doi: https://doi.org/10.1016/j.jinorgbio.2012.09.012
29. Vásquez, V. Z. C., Özcan, M., Kimpara, E. T. (2009). Evaluation of interface characterization and adhesion of glass ceramics to commercially pure titanium and gold alloy after thermal- and mechanical-loading. Dental Materials, 25 (2), 221–231. doi: https://doi.org/10.1016/j.dental.2008.07.002
30. Özcan, I., Uysal, H. (2005). Effects of silicon coating on bond strength of two different titanium ceramic to titanium. Dental Materials, 21 (8), 773–779. doi: https://doi.org/10.1016/j.dental.2005.01.014
31. Zinelis, S., Tsetsekou, A., Papadopoulos, T. (2003). Thermal expansion and microstructural analysis of experimental metal-ceramic titanium alloys. The Journal of Prosthetic Dentistry, 90 (4), 332–338. doi: https://doi.org/10.1016/s0022-3913(03)00493-1
32. Nabavi, H. F., Aliofkhazraei, M., Rouhaghdam, A. S. (2017). Electrical characteristics and discharge properties of hybrid plasma electrolytic oxidation on titanium. Journal of Alloys and Compounds, 728, 464–475. doi: https://doi.org/10.1016/j.jallcom.2017.09.028
33. Froes, F. H., Eylon, D., Eichelman, G. E., Burte, H. M. (1980). Developments in Titanium Powder Metallurgy. JOM, 32 (2), 47–54. doi: https://doi.org/10.1007/bf03354547
34. Curran, J. A., Clyne, T. W. (2006). Porosity in plasma electrolytic oxide coatings. Acta Materialia, 54 (7), 1985–1993. doi: https://doi.org/10.1016/j.actamat.2005.12.029
35. Gu, Y., Ma, A., Jiang, J., Li, H., Song, D., Wu, H., Yuan, Y. (2018). Simultaneously improving mechanical properties and corrosion resistance of pure Ti by continuous ECAP plus short-duration annealing. Materials Characterization, 138, 38–47. doi: https://doi.org/10.1016/j.matchar.2018.01.050
36. Lederer, S., Lutz, P., Fürbeth, W. (2018). Surface modification of Ti 13Nb 13Zr by plasma electrolytic oxidation. Surface and Coatings Technology, 335, 62–71. doi: https://doi.org/10.1016/j.surfcoat.2017.12.022
37. Simka, W., Sadkowski, A., Warczak, M., Iwaniak, A., Dercz, G., Michalska, J., Maciej, A. (2011). Characterization of passive films formed on titanium during anodic oxidation. Electrochimica Acta, 56 (24), 8962–8968. doi: https://doi.org/10.1016/j.electacta.2011.07.129
38. Wei, D., Zhou, Y., Jia, D., Wang, Y. (2008). Chemical treatment of TiO2-based coatings formed by plasma electrolytic oxidation in electrolyte containing nano-HA, calcium salts and phosphates for biomedical applications. Applied Surface Science, 254 (6), 1775–1782. doi: https://doi.org/10.1016/j.apsusc.2007.07.144
39. Wei, D., Zhou, Y., Jia, D., Wang, Y. (2007). Characteristic and in vitro bioactivity of a microarc-oxidized TiO2-based coating after chemical treatment. Acta Biomaterialia, 3 (5), 817–827. doi: https://doi.org/10.1016/j.actbio.2007.03.001
40. Wei, D., Zhou, Y., Wang, Y., Jia, D. (2007). Characteristic of microarc oxidized coatings on titanium alloy formed in electrolytes containing chelate complex and nano-HA. Applied Surface Science, 253 (11), 5045–5050. doi: https://doi.org/10.1016/j.apsusc.2006.11.012
41. Ramazanova, Z. M., Zamalitdinova, M. G. (2020). Study of the Properties of Qxide Coatings Formed on Titanium by Plasma Electrolytic Oxidation Method. Eurasian Chemico-Technological Journal, 22 (1), 51. doi: https://doi.org/10.18321/ectj930
42. Wheeler, J. M., Collier, C. A., Paillard, J. M., Curran, J. A. (2010). Evaluation of micromechanical behaviour of plasma electrolytic oxidation (PEO) coatings on Ti–6Al–4V. Surface and Coatings Technology, 204 (21-22), 3399–3409. doi: https://doi.org/10.1016/j.surfcoat.2010.04.006
43. Khorasanian, M., Dehghan, A., Shariat, M. H., Bahrololoom, M. E., Javadpour, S. (2011). Microstructure and wear resistance of oxide coatings on Ti–6Al–4V produced by plasma electrolytic oxidation in an inexpensive electrolyte. Surface and Coatings Technology, 206 (6), 1495–1502. doi: https://doi.org/10.1016/j.surfcoat.2011.09.038
44. Yerokhin, A. L., Leyland, A., Matthews, A. (2002). Kinetic aspects of aluminium titanate layer formation on titanium alloys by plasma electrolytic oxidation. Applied Surface Science, 200 (1-4), 172–184. doi: https://doi.org/10.1016/s0169-4332(02)00848-6
45. Shi, M., Li, H. (2016). The effect of complexing agent on Ti alloy micro-arc oxidation(MAO) coatings in Ca-P electrolyte. Protection of Metals and Physical Chemistry of Surfaces, 52 (5), 900–909. doi: https://doi.org/10.1134/s2070205116050233
46. Shabani, M., Zamiri, R., Goodarzi, M. (2015). Study on the Surface Modification of Titanium Alloy by Nanostructure TiO2 Grown Through Anodic Oxidation Treatment. Austin Chemical Engineering, 2 (1), 1015.
47. Xue, W., Wang, C., Chen, R., Deng, Z. (2002). Structure and properties characterization of ceramic coatings produced on Ti–6Al–4V alloy by microarc oxidation in aluminate solution. Materials Letters, 52 (6), 435–441. doi: https://doi.org/10.1016/s0167-577x(01)00440-2
48. Sobol', O. V., Shovkoplyas, O. A. (2013). On advantages of X-ray schemes with orthogonal diffraction vectors for studying the structural state of ion-plasma coatings. Technical Physics Letters, 39 (6), 536–539. doi: https://doi.org/10.1134/s1063785013060126
49. Klopotov, A. A., Abzaev, Yu. A., Potekaev, A. I., Volokitin, O. G. (2012). Osnovy rentgenostrukturnogo analiza v materialovedenii. Tomsk: Izd-vo TGASU, 275.

50. Troughton, S. C., Nominé, A., Dean, J., Clyne, T. W. (2016). Effect of individual discharge cascades on the microstructure of plasma electrolytic oxidation coatings. Applied Surface Science, 389, 260–269. doi: https://doi.org/10.1016/j.apsusc.2016.07.106
51. Clyne, T. W., Troughton, S. C. (2018). A review of recent work on discharge characteristics during plasma electrolytic oxidation of various metals. International Materials Reviews, 64 (3), 127–162. doi: https://doi.org/10.1080/09506608.2018.1466492
52. Belozerov, V., Mahatilova, A., Sobol', O., Subbotina, V., Subbotin, A. (2017). Improvement of energy efficiency in the operation of a thermal reactor with submerged combustion apparatus through the cyclic input of energy. Eastern-European Journal of Enterprise Technologies, 2 (5 (86)), 39–43. doi: https://doi.org/10.15587/1729-4061.2017.96721

Quenched and tempered steels are needed for highly-stressed structures in military and non-military equipment. This paper was written for studying the structure and properties (hardness and impact energy absorbed) of medium-carbon and carbon-manganese steels before and after Quench+Temper and Double Quenched+Tempered. Because water is cheap and easy to control, it was used as a quenching medium. This study compares the hardness and impact energy absorbed of quenched plus tempered and double quenched plus tempered steels. The results showed that double quenched plus tempered steel hardness was higher than in quenched plus tempered steels. Besides, the grain structure is refiner than that of quenched plus tempered steel. The taking of the austenite temperature and holding time is essential because of the hardness at the end of the quenching process. The study aims to obtain hardness and impact energy from quenching+tempering and double quenching+tempering of medium-carbon and carbon-manganese steel for armor steel. In the first step, five specimens were heated at 900 °C (held for 30 minutes), cooled in freshwater and produced Q900 Steel. Then, these specimens were heated at 750 °C, 800 °C, 850 °C, and 900 °C, held for 30 minutes and provided Q900+750 Steel, Q900+800, Q900+850 Steel, and Q900+900 Steel. These specimens were tempered at 150 °C (held for 30 minutes) and produced Q900+750&T Steel, Q900+800&T Steel, Q900+850&T Steel, Q900+900&T Steel. Martensite reached the cooling period 357 °C to 182 °C, tempered at 150 °C (held for 30 minutes). Hardness for double-quenching and tempering is higher than for conventional. The maximum impact energy of double-quenching and tempering heat treatment of Q900+850&T steel is suitable for armor steel used

Keywords: austenitizing, coarsening, compacting, embrittlement, hardening, holding, quenching, refining, softening, tempering

UDC 620
DOI: 10.15587/1729-4061.2020.214223

COMPARISON OF THE STRUCTURE AND PROPERTIES BETWEEN SINGLE QUENCH+TEMPER AND DOUBLE QUENCH+TEMPER OF MEDIUM-CARBON AND CARBON-MANGANESE STEEL

Yurianto Yurianto
Doctor of Technical Sciences, Associate Professor*
E-mail: yurianto_narimin@yahoo.com
Sulardjaka Sulardjaka
Doctor of Technical Sciences, Associate Professor, Lecturer*
E-mail: sulardjaka@lecturer.undip.ac.id
Susilo Adi Widyanto
Doctor of Technical Sciences, Associate Professor*
E-mail: susiloadiw@gmail.com
Padang Yanuar
Magister of Technical Sciences, Lecturer
Department of Mechanical Engineering
Semarang State Polytechnic
Jl. Prof. Sudarto, SH, Semarang, 50275,
Central of Java, Indonesia
E-mail: padang.yanuar@polines.ac.id
*Department of Mechanical Engineering
Diponegoro University
Jl. Prof. Sudarto, SH, Semarang, 50275,
Central of Java, Indonesia

Received date 01.09.2020
Accepted date 13.10.2020
Published date 30.10.2020

1. Introduction

In Indonesia, medium-carbon and carbon-manganese steels are the raw materials for military equipment (e. g., main battle tank body, etc.) and commercial users (e. g., pressure vessel, chain conveyor, etc.). However, because of the difficulty of quenching and tempering on 1.500×2,000 mm plates, mechanical properties were inconsistent. This means the mechanical properties generated between the first, second, and next batches are not consistent. This results in non-uniform product characteristics, so the market's selling value cannot compete with other steel industries. Also, the hardness and impact energy (very important in armored steel products) are not uniform.

Medium-carbon and carbon-manganese steels are the raw materials for armored steel. However, due to the difficul-